J Appl Electrochem (2017) 47:1127–1136
DOI 10.1007/s10800-017-1107-9

RESEARCH ARTICLE

A pore-structured Si alloy anode using an unzipping polymer for a lithium ion battery

Haeyoung Choi[1] · Panjin No[1] · You-Jin Lee[1] · Jeong-Hee Choi[1]

Received: 26 March 2017 / Accepted: 13 July 2017 / Published online: 24 July 2017
© Springer Science+Business Media B.V. 2017

Abstract Polymethyl methacrylate (PMMA), which has the thermal property of unzipping, was used as a pore-forming agent during electrode fabrication to solve the chronic volume expansion problem in silicon (Si) anodes for lithium ion batteries (LIBs). PMMA-treated Si alloy electrodes have low volume expansion resulting in low deformation during lithiation. To maximize the effect of a porous structure, the pore diameter in the electrode was controlled. The best cycling stability was obtained when using 10 μm diameter PMMA. After 100 cycles at the 0.5-C rate a bare electrode retained 39% capacity, whereas an electrode using 10 μm diameter PMMA retained 62%. The outstanding capacity retention obtained from porous electrodes originated from the optimized porous architecture. Furthermore, PMMA-treated electrodes provide the lowest resistance in a cell by facilitating fast electron and ion transport, enhancing battery performance. Hence, for cycle-guaranteed Si-based LIBs these porous electrodes could provide an alternative or supplementary structure to other more complex manufacturing processes.

Graphical Abstract Schematic diagram of the porous electrode fabrication process using polymethyl methacrylate (PMMA) and the electrochemical test results obtained from the 3-dimensional structures.

✉ Jeong-Hee Choi
dodgers@keri.re.kr

[1] Battery Research Center, Korea Electrotechnology Research Institute, Changwon-si, Gyeongnam, South Korea

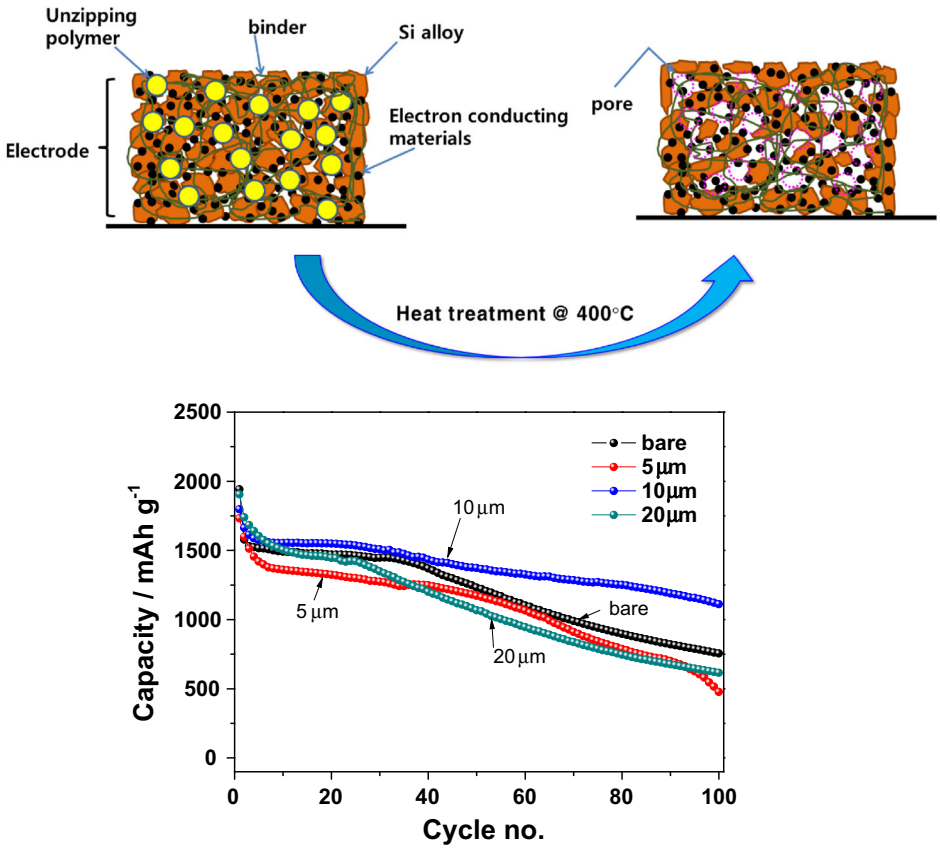

Keywords Porous-structured electrode · PMMA · PAI · Imidization · Unzipping polymer

1 Introduction

Lithium ion batteries (LIBs) have attracted attention as large-scale power sources for energy storage systems (ESSs) and electric vehicles (EVs). Batteries for these applications must have high power/energy density and a long cycle life. To achieve the desired performance, various materials have been investigated for use in positive and negative electrodes. A binder, separator, substrate, and electrolyte are also included, but the performance of LIBs is critically dependent on the properties of the electrodes [1, 2]. Thus, the electrode materials and their structural/morphological characteristics are important factors determining the performance of LIBs.

Graphite is one of the most commonly used anode materials in LIBs, due to its relatively low cost and long cycle life. However, graphite anodes have some issues with low gravimetric and volumetric capacity (LiC_6, 372 mAh g^{-1}, 804 Ah L^{-1}), limiting the energy density of LIBs. In contrast, silicon (Si) is an alternative anode material for LIBs that can store 10 times more lithium (Li, as $Li_{22}Si_5$, 4200 mAh g^{-1}; 8343 Ah L^{-1}) than current commercial graphite anodes [3]. Additionally, Si has a low electrochemical potential for lithiation/delithiation, high natural abundance, and low toxicity, making it an attractive candidate for LIB electrodes [4]. However, the commercial use of Si-based anodes is still hindered by two major challenges: their low electric conductivity, leading to poor rate capability, and their huge volume change (400%) during the charge–discharge cycling process, resulting in the degradation of electrodes and rapid loss of capacity [4, 5]. As this has impeded the practical application of Si as an anode material, numerous studies have explored the intrinsic properties of Si upon the lithiation and delithiation associated with large volumetric changes [3].

Structural modification of the electrode is one effective method for mitigating the volume change and improving cycling performance, enhancement of ionic and electric conductivity, accommodation of volumetric changes, and prevention of particle agglomeration have been demonstrated. To increase the stability of Si anodes, several structural modification methods have been developed, including nanostructuring, atomic layer deposition (ALD), and molecular layer deposition (MLD) [3]. A range of Si anode types can be formed

using these processes, which provide effective protection against capacity decay. For example, ALD and MLD alucone-coated Si anodes have shown sustainable cycling performance, with a high coulombic efficiency above 99.9% [3]. However, more simple process for fabricating LIBs than using these methods is required, as the current techniques are complicated and expensive.

In this study, we developed a three-dimensional (3D) porous electrode using a simple structure modification method that suppresses severe volumetric changes in the electrode and improves cyclic performance. The results are discussed by comparison with the experimental data obtained from morphology and electrochemical analyses, to elucidate the impact of a porous structure on the cycling behavior and interfacial physics of Si alloy anodes.

2 Experimental

2.1 Materials

Si alloy used as the Si-based active material in this study was provided by Iljin Electric Co. Ltd. (Republic of Korea). The Si alloy contained about 86.6 at.% Si (~48.6 wt% Si) and Al–Ti–Fe matrix phase. The particle size was round 2–10 μm. This inactive metal matrix helped sustain the stress generated during the lithiation/delithiation of the Si alloy material and enhanced the electronic conductivity of the Si alloy electrode [6, 7]. The active material was synthesized using arc melting followed by the single roll solidification method, as previously reported [6, 7].

2.2 Electrode fabrication for the study of PAI binder properties

Polyamideimide (PAI)-binder-based electrodes were prepared by mixing 86.6 wt% Si–Al–Ti–Fe matrix phase active material, 3.4 wt% Ketjen black (KB) as a conducting agent, and 10 wt% PAI as a precursor for the PI binder, all dissolved in *N*-methyl-2-pyrrolidone (NMP). The resulting slurry was coated on copper foil (thickness = 10 μm) with a packing density of 0.7–1.0 g cm^{-3}, a loading level of 1.0 g cm^{-2}, and dried at 100 °C for 30 min in a forced convection oven. After evaporating the NMP solvent, the electrode was heat treated at temperatures of 250, 300, 350, and 400 °C, for 1 h under an argon atmosphere to imidize the PAI to polyamide (PI).

2.3 Electrode fabrication for the study of 3-dimensional structure with PMMA

Porous-structured electrodes were prepared using polymethyl methacrylate (PMMA) unzipping polymers of various particle sizes to control the vacancy size in the electrode. The bulk density of the PMMA was 0.5–0.6 g cm^{-3} and the particle sizes used were 5, 10, and 20 μm (S50, S100, and S200, SUNJIN Corp.). The diameters of PMMAs were revealed as mean values because all PMMAs used in this study had size distribution with Gaussian form.

PMMA-treated porous electrodes were prepared by mixing 86.6 wt% Si–Al–Ti–Fe alloy active material, 3.4 wt% KB as a conducting agent, 10 wt% PAI as a precursor for the PI binder, and additional 14 wt% PMMA as a pore-forming agent, all dissolved in NMP. The resulting slurry was coated on copper foil (thickness = 10 μm) with a packing density of 0.7–1.0 g cm^{-3} and dried at 100 °C for 30 min in a forced convection oven. After evaporating the NMP solvent, the electrode was heat treated at 400 °C for 1 h under an argon atmosphere to unzip the PMMA pore-forming agent and imidize the PAI to PI. A bare electrode was fabricated by the same procedure without using PMMA particles.

2.4 Electrochemistry

Electrochemical measurements of bare and porous electrodes were conducted with CR2032 coin cells, using metallic Li foil as a counter and Celgard 2325 as a separator. The electrolyte consisted of a 1.15 M solution of $LiPF_6$ in ethylene carbonate (EC), diethylene carbonate (DEC), and ethyl methyl carbonate (EMC) (EC/EMC/DEC ratio = 3/5/2) containing 5 wt% fluoroethylene carbonate (FEC) and 2 wt% vinylene carbonate (VC). The cells were aged overnight at room temperature and electrochemically tested using a WonA Tech instrument (Standard type WBCS3000S Automatic Battery Charge/Discharge Test System). In the coin-type cell tests, the first cycle was operated for formation at a constant current–constant voltage (CC–CV) of 0.1 C (150 mA g^{-1}) to 0.005 V with 0.01 C (15 mA g^{-1}) cut-off during the lithiation process, and CC of 0.1 C to 0.005–1.5 V during the delithiation process. The protocol used for the cycling was similar to that of the formation program, which was applied with 0.5 C (750 mA g^{-1}).

2.5 Characterizations

The morphology and elements of the samples were investigated using a field emission scanning electron microscope (FE-SEM, S-4800; Hitachi) working at 10 kV. Thermogravimetric analysis (TGA) (SDT Q600; TA Instruments) was performed at a heating rate of 5 °C min^{-1}. The porosity and pore diameter of the 3D electrode were determined using a mercury porosimeter (Autopore IV 9520; Micromeritics). The charge transfer resistances of

the cells were obtained using an AC impedance technique over the frequency range 0.01–100 kHz using a Solartron SI 1260 frequency response analyzer combined with an SI 1287 electrochemical interface at a constant potential of 10 mV and the cell potential had kept around 0.15–0.18 V (vs. Li/Li^+) during the measurements.

The adhesion strengths at the interface between the anode composite and current collector, and within the middle point of the anode composite, were measured using a surface and interfacial cutting and analysis system (SAICAS). For this measurement, a boron nitride blade (width = 1 mm) with a shear angle of 45°, a rake angle of 20°, and a clearance angle of 10° was used. During the test, the blade moves horizontally at 2 μm s^{-1}. In cutting mode, the blade also moves vertically, with a force of 0.5 N, until it reaches the Cu current collector; subsequently, in the peel mode, the vertical force is reduced from 0.5 to 0.2 N to prevent further vertical movement. The adhesion strength can be calculated by averaging the horizontal forces during the peel mode, divided by the blade width. At least three measurements were conducted with each sample to obtain more reliable results.

3 Results and discussion

3.1 Adhesion properties of PAI

In an attempt to overcome the mechanical disintegration of Si-based anodes caused by the large variation in volume during Li^+ insertion and extraction, this study considered the addition of a PAI binder with superior mechanical and thermal properties to Si alloy-based anodes. Although the PAI binder has been found to react with Li ions electrochemically during the first charge, capacity fading of the Si anode is alleviated significantly by the high tensile strength of PAI [8, 9].

Furthermore, different heat treatment temperatures cause the PAI in the electrode to have very different adhesion strength and physical hardness, which affects the degree of imidization. According to Cho et al. PAI has low hardness and good adhesion below 350 °C, because imidization will generally not occur and the chemical structure does not change substantially up to 350 °C. On the other hand, the hardness is enhanced when it is cured over 350 °C while the adhesion strength decreases [10]. Therefore, if PAI is used as a binder, a prior step to find the optimum curing conditions should be undertaken.

The TGA results are shown in Fig. 1. The PAI polymer began to decompose from 400 °C and significant weight loss was observed at temperatures greater than 560 °C. Hence, it could be inferred that the curing temperature should be below 400 °C.

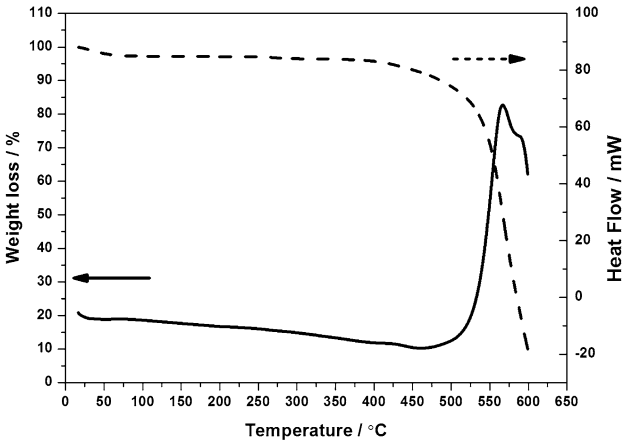

Fig. 1 Thermogravimetric analysis (TGA) results of polyamideimide (PAI) binder. *Straight line* for weight loss and *dot line* for heat flow

A charge–discharge test was conducted to investigate changes in electrochemical properties with curing temperature further. Figure 2 shows the cyclic stability over a range of heat treatment temperatures. The electrode with the PAI binder delivered an initial discharge capacity of ~1821 mAh g^{-1} and remained stable for up to 40 cycles in the range ~1500 mAh g^{-1} at 400 °C, while the others decreased drastically.

To support the results of the electrochemical test, and in particular to elucidate the role of the binder in binding particles, we measured the adhesion strength of the electrodes using SAICAS. The adhesion strength (P) of electrodes can be calculated by measuring the horizontal force ($F_{H,Peeling}$) during peeling at a constant rate, then dividing the average horizontal force by the width of the blade (w) of SAICAS, as shown in Eq. (1) [10, 11].

$$P = F_{H,Peeling}/w \ \left(\mathrm{kN\ m^{-1}}\right). \quad (1)$$

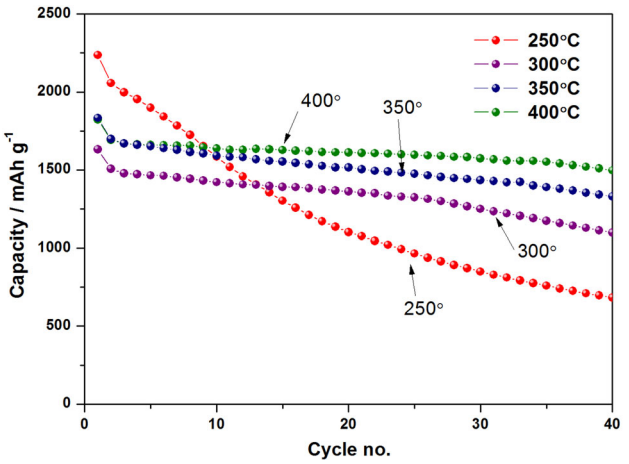

Fig. 2 Cyclic performance of silicon (Si) alloy electrodes at various curing temperatures. (Color figure online)

As shown in Fig. 3a, the adhesion at the interface between the anode composite and the current collector remained similar at around 0.5–0.6 kN m^{-1}, regardless of curing temperature. However, as shown in Fig. 3b, significant differences were observed at the midpoint of the anode. This indicates that the adhesion strength at the midpoint of the anode composite was stronger at 400 °C than at other curing temperatures. This implies that PAI adhesion strength of itself decreased according to imidization reaction, but it might be changed when it mixed up with other materials; especially at the midpoint of the anode composite. Therefore, in this study, we could conclude that the drastic capacity fading in low curing temperature under 350 °C might be attributed to a decrease in the adhesion strength among other materials at the midpoint of the anode composite and a decline of hardness. This result is consistent with the electrochemical performance shown in Fig. 2. It can therefore be concluded that

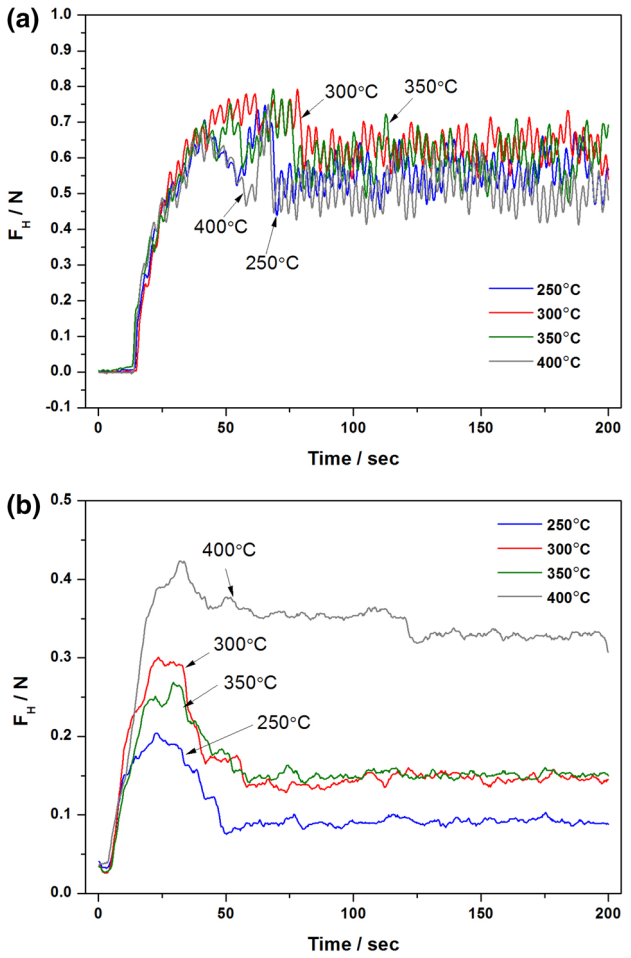

Fig. 3 Adhesion strength at the interface between the anode composite and current collector (**a**) and at the midpoint of the anode composite (**b**) measured by a surface and interfacial cutting and analysis system (SAICAS). (Color figure online)

improved adhesion strength at the midpoint of the anode composite leads to better retention of discharge capacity during cycling, especially when the electrode is cured at 400 °C.

SEM analysis was conducted to confirm surface morphologies after charge–discharge. As shown in Fig. 4, the electrode surface had wide cracks, caused by repetitive expansion and shrinkage during the electrochemical test, which could have induced the poor cyclic performance.

To confirm the swelling status which could cause decrease of cycle property, the thicknesses of the electrodes were measured. As shown in Table 1, the electrode thickness change ratio decreased at higher curing temperatures; values of 166 and 33% of the first charge and discharge state at 400 °C were observed, respectively. This seems to be closely related to the imidizing effect which might cause shrinkage of the electrodes. Therefore, we could confirm the imidization and it could deduce that the formation of an imidized electrode could force in adhesion and curing at 400 °C that was more effective than at the other temperatures (Table 2).

3.2 Properties of PMMA-treated porous electrodes

An appropriate PAI curing temperature was found to be 400 °C. However, poor cyclic properties caused by volume expansion were still observed. In this section, we suggest a specific structured electrode that has buffering cavities created by an unzipping polymer to mitigate huge volumetric changes and improve cyclic performance. The process instruction for unzipping system of polymer has been well described in the previous literature [12]. Figure 5 shows a schematic diagram of the porous electrode fabrication process using PMMA to control the severe volume expansion of the Si alloy electrode. PMMA was used to generate pores inside the electrode because of its unique thermal properties. It was expected that the pores would play a crucial role in buffering the volume of the layer during charge and discharge. SEM images of porous electrodes with PMMA particles of different sizes are shown in Fig. 6, confirming the morphologies of the fabricated electrode prior to cycling. As expected, the generated pores had spherical shapes and were homogeneously distributed in the electrodes.

Mercury intrusion porosimetry (MIP) and an electrochemical test were performed to investigate the correlation between porous structure and cycle stability. Four kinds of sample were prepared, treated with 5, 10, and 20 μm PMMA, and a bare Si alloy electrode was also investigated for comparison; as shown in Fig. 7, the porosity order was 20 μm > 10 μm > 5 μm > bare. The bare electrode had ~47.5% porosity, which increased to ~68% with 20 μm PMMA. Porosity seemed to be related to cyclability due to

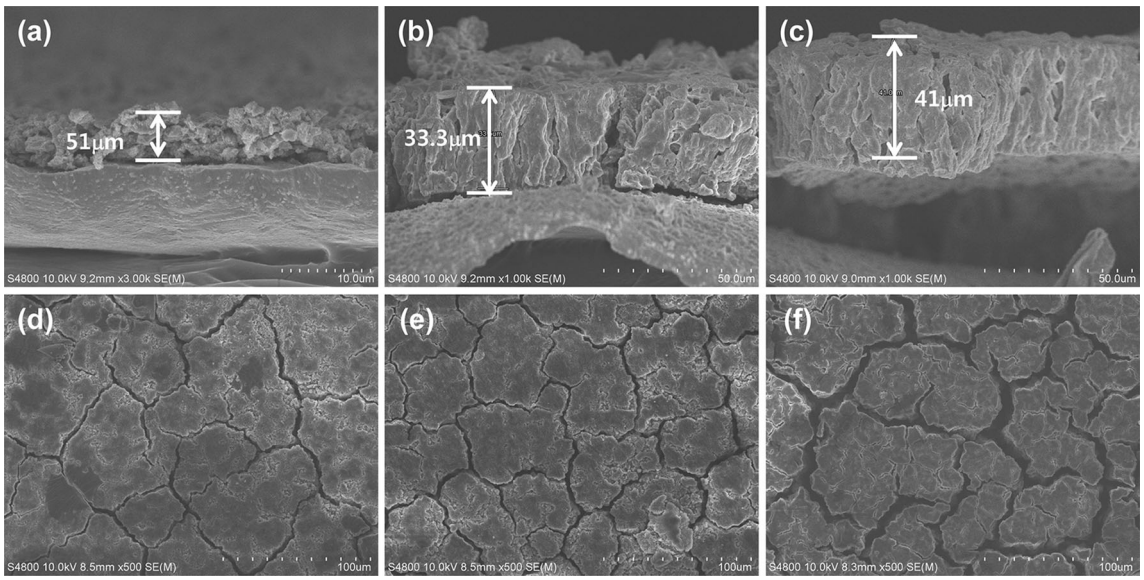

Fig. 4 **a–c** Scanning electron microscope (SEM) images of a cross section of a sample cured at 400 °C after **a** first cycle lithiation, **b** 100th cycle lithiation, **c** 100th cycle delithiation, and **d–f** SEM images of surfaces of each of **a–c**

Table 1 Thickness changes of electrodes constructed with various curing temperature

Curing temp. (°C)	Thickness after 1st charging (fresh/lithiated)	Percent ratio of thickness change (%)	Thickness after 1st discharging (fresh/delithiated)	Percent ratio of thickness change (%)
250	9/27	200	8/15	87
300	9/26	188	9/12	33
350	8/23	187	9/12	33
400	9/24	166	9/12	33

Table 2 Thickness changes of electrodes constructed with PMMA of various diameters

PMMA size (μm)	First discharge (lithiated)		First charge (delithiated)		ICE (%)	Capacity retention
	Thickness change (%)	Density (g cm^{-3})	Thickness change (%)	Density (g cm^{-3})		At 100th cycle (%)
Bare	166	0.97	33	1.01	86.3	38.9
5	113	1.05	32	1.01	86.5	27.6
10	102	0.61	23	0.55	87.6	61.8
20	32	0.33	12	0.38	78.6	32.3

PMMA, polymethyl methacrylate; ICE, initial coulombic efficiency; bare, cured at 400°C, and non-porous sample

mechanical structure durability, which was in turn strongly related to volume expansion. The capacity to accommodate volume expansion increased with increasing pore size; however, excessive empty spaces promoted low structural stability between electrode materials, even though the volume expansion was accommodated sufficiently, leading to an increase in internal resistance, as observed for the 20 μm pore size electrode. In contrast, structure contortion can be generated by high strain in the electrode after the lithiation process when the electrode pores are below 5 μm in size. These behaviors would reduce cyclability. This is consistent with the electrochemical performance shown in Fig. 8. Figure 8a compares the cyclic performance of the Si alloy anodes. As illustrated in Fig. 8a and Table 1, after 100 cycles the electrode with the bare Si alloy showed a drastic capacity loss, with capacity retention of just 38.9%

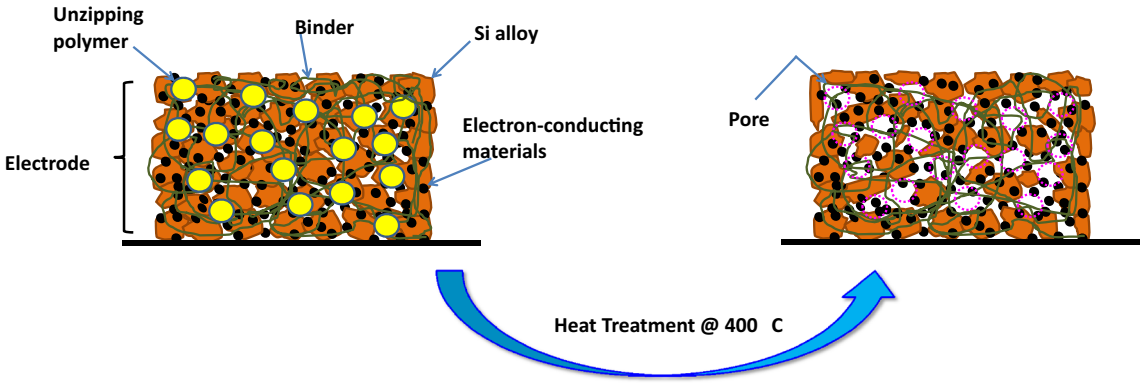

Fig. 5 Schematic diagram of the porous electrode fabrication process using polymethyl methacrylate (PMMA)

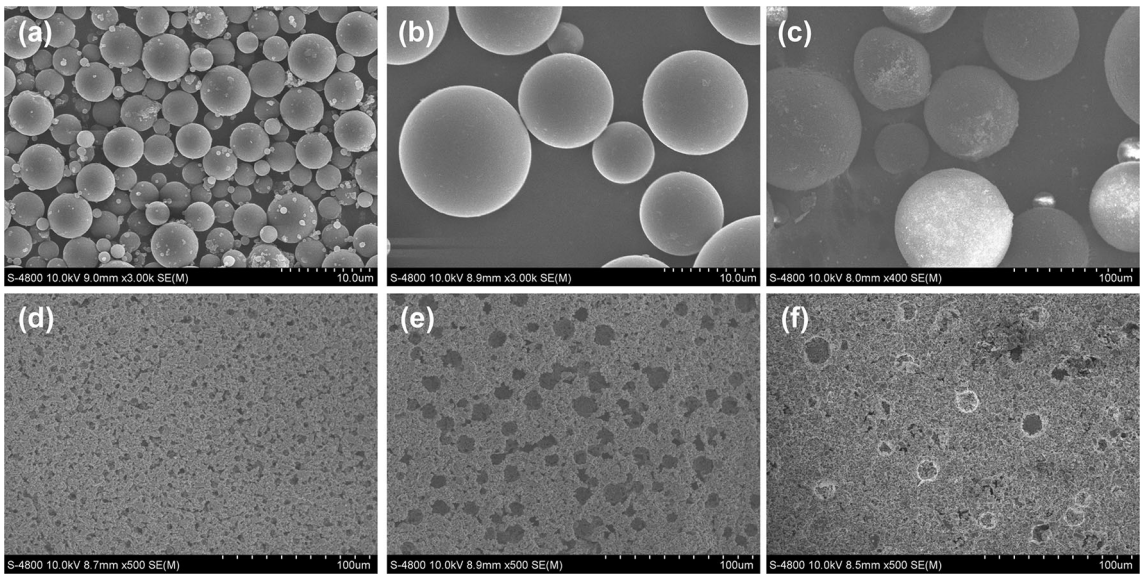

Fig. 6 SEM images of PMMA powders with diameters of **a** 5 μm, **b** 10 μm, and **c** 20 μm; **d**–**f** are the three-dimensional electrodes constructed from **a**–**c**

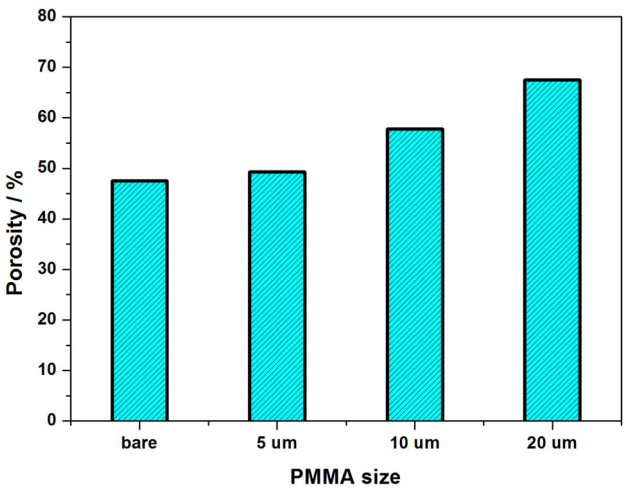

Fig. 7 Porosity measurements of porous electrodes constructed using pmma of various diameters

and charge capacity decreasing to 755.5 mAh g^{-1}. However, the cyclability of the electrode with the 10 μm diameter PMMA improved significantly, maintaining a charge capacity as high as 1111.1 mAh g^{-1} after 100 cycles, i.e., a capacity retention of 61.8%. Figure 8b, c compare the charge–discharge curves of bare Si alloy electrodes and porous electrodes treated with 10 μm PMMA. The discharge potential plateaus of the bare Si alloy electrode showed obvious decreases, indicating that polarization increased significantly due to pulverization and fracture of the electrode during the charge–discharge cycling processes. However, the potential plateaus of lithiation/delithiation with the porous-structured Si alloy electrode showed less structural change during the cycling process, indicating a stable electrode structure [13]. These improved electrochemical performances can be attributed to the buffer volume structure formed by the unzipping

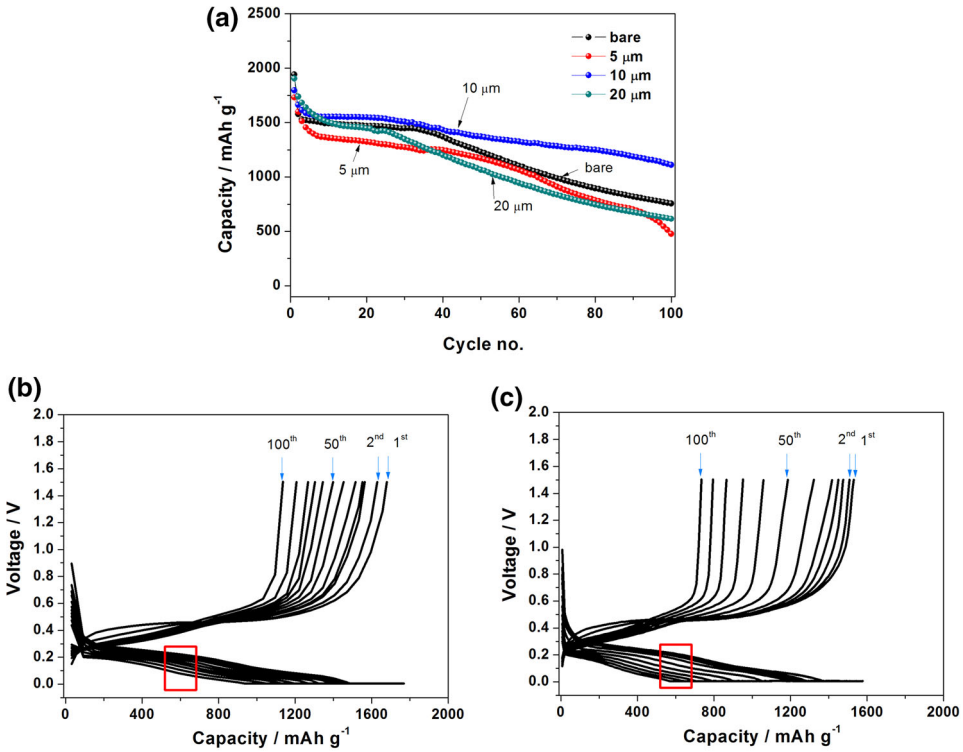

Fig. 8 Electrochemical test results; **a** cyclic performance with various types of electrode, **b** charge–discharge voltage profile of a bare Si alloy electrode, and **c** charge–discharge voltage profile of a porous-structured Si alloy electrode constructed with 10 μm diameter PMMA; **b**, **c** exclude formation cycle. (Color figure online)

polymer PMMA, which mitigates severe volume expansion during the charge–discharge process. It is therefore beneficial to maintain an electrode structure that minimizes pulverization and fracture during cycling processes, as illustrated schematically in Fig. 5.

SEM samples were prepared from 10 μm PMMA-treated electrode after 100 cycles to confirm the change in morphology after PMMA treatment. Figure 9 shows SEM images of the electrode surface and the cross section after delithiation. The 10 μm PMMA-treated electrode had a more robust structure compared to the bare Si alloy electrode in Fig. 4c, g; the porous electrode had less cracks and fractures than the bare Si alloy electrode. The thickness of the 10 μm PMMA-treated electrode was measured from SEM observations to investigate the thickness change further, as shown in Fig. 9b after the first cycle, with detailed values listed in Table 1. The thickness change after the first cycle for the bare Si alloy electrode was around 166%; however, this value decreased to 32% for the 20 μm PMMA-treated electrode. Hence, while the bare Si alloy electrode does not prevent volume expansion during complete lithiation, it does allow for a porous electrode to accommodate expansion of the lithiated Li_xSi alloy.

Electrochemical impedance spectroscopy (EIS) measurements were carried out to elucidate the effect of the macropore-structured electrode as a volume buffer layer. The EIS data were analyzed based on the equivalent circuit shown in Fig. 10a. In general, R_s refers to the uncompensated resistance, which includes a number of contributions: particle–particle contact resistance, electrolyte resistance, and the resistance between the electrode and the current collector. R_{ct} refers to the charge transfer resistance associated with interfacial electrochemical reactions, which is related to the electrochemical reaction at the electrode–

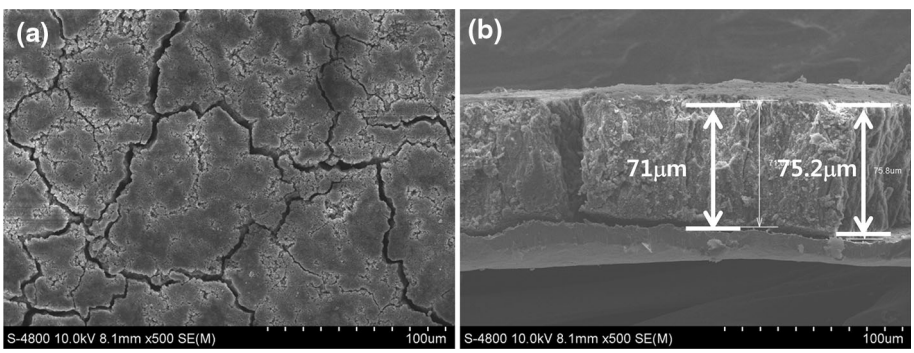

Fig. 9 SEM images of the multi-pore electrode created using the unzipping polymer PMMA of diameter 10 μm, which was delithiated at the first cycle. **a** Surface. **b** Cross section

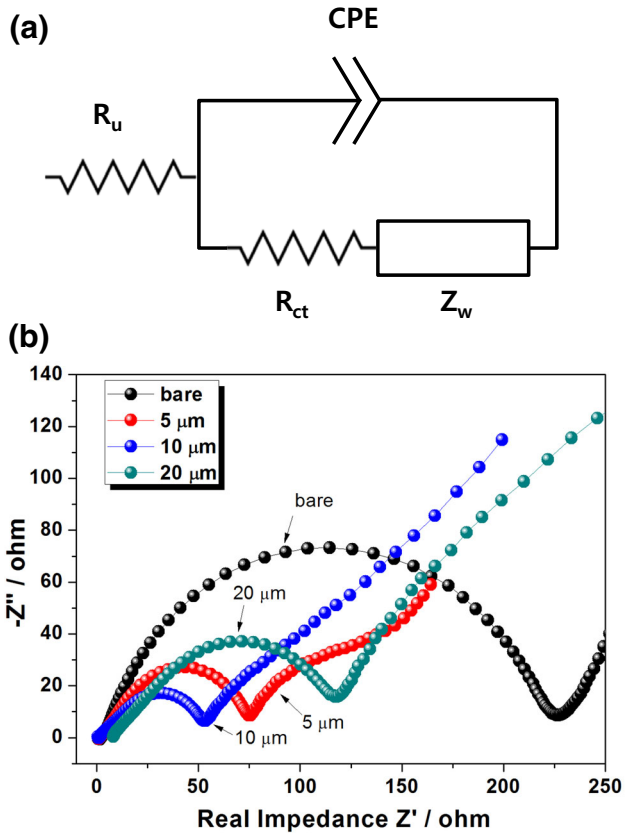

Fig. 10 **a** Equivalent circuit model and **b** Nyquist plots of first-charge electrode (measured in the frequency range 0.01–100 kHz). (Color figure online)

electrolyte interface and the particle–particle contact. CPE represents the dispersion effects caused by inhomogeneity, such as impurities and defects in the crystals [14–16]. Figure 10b shows typical Nyquist plots, which consist of semicircles in the high-to-medium frequency region and their inclined line in the low-frequency region. The semicircle is indicative of the charge transfer resistance (R_{ct}) associated with the interfacial electrochemical reactions. This can be attributed to the Warburg impedance, which is relevant to the Li-ion diffusion in a Si alloy electrode, considering the impedance derived from the electrolyte (R_s) and the constant phase element used instead of double-layer capacitance to consider the surface roughness of the particle. The values for R_s are similarly below $\sim$1.6 Ω for up to 10 μm pores, but increased to 8.09 Ω at the 20 μm pore size. In other words, the conductivity decreased with excessive space and the values for R_{ct} decreased unexpectedly up to 53.22 Ω for the 10 μm pores, indicating enhancement of both the electron and coupled Li^+ transfer rates into the Si alloy electrode. In particular, the 10 μm pores exhibited values below 1/4 R_{ct} compared with those of the bare electrode. The above electrochemical results confirm that the macropore-structured electrode effectively improved cyclic performance by controlling the volume change of the electrode.

4 Conclusion

In this study, a Si alloy electrode was prepared using a PAI binder and its electrochemical properties and curing temperature were investigated to assess the potential of PAI for use as a binder for Li-ion batteries. It was established that 400 °C was an appropriate temperature for curing. A porous-structured Si alloy electrode using PMMA as a pore-forming agent was fabricated to alleviate volume expansion for improved cyclability. To obtain the best electrochemical properties, PMMA-treated electrodes with macropore distributions that varied according to the diameter of the applied PMMA beads were fabricated. In contrast to the bare electrode, the 10 μm PMMA-treated electrode showed the best cyclic stability, exhibiting a high specific capacity of 1135 mAh g^{-1} after 100 cycles at a current density of 750 mAh g^{-1}. This microstructurally controlled electrode therefore relieves mass stress in the electrode and provides the void space necessary to mitigate volume expansion. These results indicate that this approach can facilitate fast electron and ion transport, provide more active sites, and allow volume changes during Li-ion insertion. The results are also consistent with those of our previous study, which used polystyrene as an unzipping pore-forming agent; electrode performance was improved by the presence of macropores in the Si alloy [7]. Porous electrodes may provide an alternative or supplementary structure to other more complicated manufacturing processes for the commercialization of cycle-guaranteed Si-based Li-ion batteries.

Acknowledgements This work was supported by the Secondary Battery R&D Program for Leading Green Industry, provided by MOTIE/KEIT [10046341, Development of a silicon negative material with a high capacity (>1600 mAh g^{-1}) and low price (<35$ kg^{-1}) for lithium secondary batteries].

References

1. Morishita M, Yamano A, Kitaoka T, Sakai H, Ojima T, Sakai T (2014) Polyamide-imide binder with higher adhesive property and thermal stability as positive electrode of 4V-class lithium-ion batteries. J Electrochem Soc 161(6):A955–A960. doi:10.1149/2.039406jes
2. Jeong G, Lee SM, Choi NS, Kim Y-U, Lee CK (2011) Stabilizing dimensional changes in Si-based composite electrodes by controlling the electrode porosity: an in situ electrochemical dilatometric study. Electrochim Acta 56(14):5095–5101. doi:10.1016/j.electacta.2011.03.071
3. Ma Y, Martinez de la Hoz JM, Angarita I, Berrio-Sanchez JM, Benitez L, Seminario JM, Son S-B, Lee S-H, George SM, Ban C,

Balbuena PB (2016) Structure and reactivity of alucone-coated films on Si and LixSiy surfaces. ACS Appl Mater Interfaces 7(22):11948–11955. doi:10.1021/acsami.5b01917
4. Lin L, Xu X, Chu C, Majeed MK, Yang J (2016) Mesoporous amorphous silicon: a simple synthesis of a high-rate and long-life anode material for lithium-ion batteries. Angew Chem Int Ed 55(45):14063–14066. doi:10.1002/anie.201608146
5. Cho J (2010) Porous Si anode materials for lithium rechargeable batteries. J Mater Chem 20(20):4009–4014. doi:10.1039/b923002e
6. Yu B-C, Kim H-Y, Park Ch, Kim SK, Sung JW, Sohn H-J (2014) Si Nano-crystallites embedded in Cu–Al–Fe matrix as an anode for Li secondary batteries. Electrochim Acta 130:583–586. doi:10.1016/j.electacta.2014.03.067
7. Lee Y-J, Hwang M, Choi H, Baek J, Baek Y-K, Choi J-H (2016) Fabrication of macroporous Si alloy anodes using polystyrene beads for lithium ion batteries. J Appl Electrochem 46(6):695–702. doi:10.1007/s10800-016-0965-x
8. Choi N-S, Yew KH, Choi W-U, Kim S-S (2008) Enhanced electrochemical properties of a Si-based anode using an electrochemically active polyamide imide binder. J Power Sources 177(2):590–594. doi:10.1016/j.jpowsour.2007.11.082
9. Alcántara R, Pedro L, Carlos P-V, José LT (2011) Anode materials for lithium-ion batteries. In: Yuan X, Liu H, Zhang J (eds) Lithium-ion batteries: advanced materials and technologies. CRC Press, New York, pp 97–146
10. Cho JH, Kong DI, Park CE, Jin MY (1998) Effect of curing temperature on the adhesion strength of polyamideimide/copper joints. J Adhes Sci Technol 12(5):507–521. doi:10.1163/156856198x00191
11. Son B, Ryou M-H, Choi J, Lee T, Yu HK, Kim JH, Lee YM (2014) Measurement and analysis of adhesion property of lithium-ion battery electrodes with SAICAS. ACS Appl Mater Interfaces 6(1):526–531. doi:10.1021/am404580f
12. An J, Ke Y, Cao X, Ma Y, Wang F (2014) A novel method to improve the thermal stability of poly(propylene carbonate). Polym Chem 5(14):4245–4250. doi:10.1039/c4py00013g
13. Liu J, Zhang Q, Wu Z-Y, Wu J-H, Li J-T, Huang L, Sun S-G (2014) A high-performance alginate hydrogel binder for the Si/C anode of a Li-ion battery. Chem Commun 50(48):6386–6389. doi:10.1039/c4cc00081a
14. Jinli Z, Jiao W, Yuanyuan L, Ning N, Junjie G, Feng Y, Wei L (2015) High-performance lithium iron phosphate with phosphorus-doped carbon layers for lithium ion batteries. J Mater Chem A 3(5):2043–2049. doi:10.1039/c4ta05186f
15. Kim J, Kim JY, Pham-Cong D, Jeong SY, Chang J, Choi JH, Braun PV, Cho CR (2016) Individually carbon-coated and electrostatic-force-derived graphene-oxide-wrapped lithium titanium oxide nanofibers as anode material for lithium-ion batteries. Electrochim Acta 199:35–44. doi:10.1016/j.electacta.2016.03.137
16. Lu H, Wu L, Xiao L, Ai X, Yang H, Cao Y (2016) Investigation of the effect of fluoroethylene carbonate additive on electrochemical performance of Sb-based anode for sodium-ion batteries. Electrochim Acta 190:402–408. doi:10.1016/j.electacta.2015.12.136